PHYSICAL REVIEW D **73,** 074006 (2006)

3D jet topography of the twisted color glass condensate

A. Adil,* M. Gyulassy,† and T. Hirano‡

Department of Physics, Columbia University, 538 West 120th Street, New York, New York 10027, USA

(Received 27 September 2005; revised manuscript received 13 February 2006; published 7 April 2006)

Independent experimental constraints on the initial condition assumed in hydrodynamics to predict collective flow in Au + Au at 200 AGeV are essential to strengthen the case for the "perfect fluid" property of deconfined quark-gluon matter. We propose a 3D jet tomographic test of possible novel initial surface geometries predicted by a color glass condensate model of initial conditions. We show that high p_T and rapidity, η, differential directed flow $v_1(p_T > 6, |\eta| > 1)$ is sensitive to the generic rapidity twist of the bulk low p_T matter in the reaction plane and can differentiate between conventional diffuse Glauber surfaces and sharper surfaces possible in some parametrizations of the color glass condensate.

DOI: 10.1103/PhysRevD.73.074006 PACS numbers: 25.75.−q, 12.38.Mh, 24.85.+p

I. INTRODUCTION

It was pointed out in Ref. [1] that the QCD matter produced in high energy noncentral $A + A$ nuclear reactions violates (*locally*) Bjorken longitudinal boost invariance in the transverse plane even if the global rapidity distribution, $dN/d\eta$, is independent of $\eta = \sinh^{-1}(p_z/m_\perp)$. The intrinsic longitudinal boost noninvariance occurs even in symmetric $A + A$ reactions because locally in the transverse $\mathbf{x}_\perp$ plane, the initial gluon density, $\rho_g(\eta, \mathbf{x}_\perp) = dN_g/d\eta d^2\mathbf{x}_\perp$, has a generic "trapezoidal" form in the rapidity variable. This peculiar structure arises in noncentral ($b > 0$) collisions because there is an asymmetry between the local number of interacting projectile and target nucleons, $\Delta\nu(\mathbf{x}_\perp; b > 0) \sim A^{1/3}$, that can vary by an order of magnitude in heavy nuclei with the transverse coordinate, $\mathbf{x}_\perp$. Since low p_T bulk matter is known to be produced proportional to the number of participating nucleons, the slope of the rapidity trapezoid varies with $\mathbf{x}_\perp$ as $d\rho/d\eta \propto \Delta\nu(\mathbf{x}_\perp; b)/2Y \sim A^{1/3}/\log s$, where $2Y = \log s$ is the rapidity gap between the projectile and target nuclei. At infinite energies this slope approaches zero, but at the Relativistic Heavy Ion Collider (RHIC) and the Large Hadron Collider (LHC) it may be large enough to be observable via 3D $(p_\perp, \phi, \eta)$ extensions [1] of jet tomography [2].

A trapezoidal rapidity asymmetry has been observed at all energies in $p + A$ reactions and it was also clearly seen in D + Au reactions at RHIC [3,4]. The data are well reproduced by phenomenological soft + hard (string + mini-jet) models such as [5–7]. However, these trapezoidal features are also well reproduced by gluon saturation models such as in the Kharzeev-Levin-Nardi (KLN) [8] implementation of the color glass condenstate (CGC) theory [9,10] of low Bjorken x parton initial conditions. Thus, one cannot differentiate between the phenomological soft + hard approach and the CGC formalism using purely bulk observables.

At RHIC the strongest support for the KLN/CGC approach is its remarkable ability to reproduce the extensive systematics of the energy, centrality and nuclear size dependence of the global p_T integrated $dN_{ch}/d\eta$. This results from a specific dependence of the saturation scale, Q_s, on $\sqrt{s}$ and A. In contrast, phenomenological soft-hard models such as HIJING failed to reproduce the systematics because the separation scale, $p_0 \sim 2$ GeV, between soft and hard parton production was assumed to be independent of those variables. An open question is how high in p_T can various k_T-factorized CGC approximations be pushed in specifying the $A + A$ initial conditions. Similarly, it is important to constrain how low in p_T can the conventional collinear factorized approximation be used. Both experimental and theoretical control over the initial conditions in $A + A$ at RHIC are essential to strengthen or refute the current case made for the discovery of new forms of matter, the strongly coupled quark gluon plasma (sQGP) and CGC, at RHIC [11–13].

Even though both approaches reproduce integrated bulk multiplicities in heavy ion collisions, they lead to significantly different bulk matter eccentricities and transverse reaction plane distributions that in turn cause different hydrodynamic and flow evolution [14]. The applicability and specific predictions of hydrodynamics concerning QCD matter at RHIC is a crucial component of the current claim that a nearly "perfect fluid" has been produced in the heavy ion experiments [12]. In order to make specific inferences about the properties of the QCD bulk using hydrodynamics, one needs to better constrain experimentally the initial conditions prevalent prior to the onset of evolution.

In this paper a new jet tomographic approach is proposed based on extending the discussion in Ref. [1] to KLN/CGC initial conditions of the sQGP bulk as well as its extrapolation to high $p_T \gg Q_s$ jet partons. The idea is to exploit the difference between the geometric distributions of jets relative to that of the bulk matter as illustrated in Fig. 1. We focus on the predicted azimuthal dependence

*Electronic address: azfar@phys.columbia.edu
†Electronic address: gyulassy@phys.columbia.edu
‡Electronic address: hirano@phys.columbia.edu

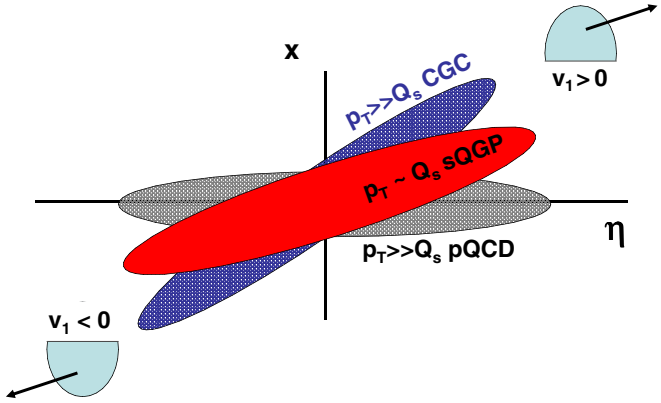

FIG. 1 (color online). Illustration of the initially twisted sQGP gluon density [1] relative to the beam axis in the (x, η) reaction plane. CGC [8], BGK [5], and HIJING [7] predict this generic low $p_T \lesssim Q_s$ locally boost noninvariant structure. Also shown are the relative rotations of the high $p_T \gg Q_s$ jet partons in the k_T factorized CGC model as well as conventional collinear factored pQCD. Jet quenching through the sQGP leads to opposite sign first azimuthal harmonic moment, $v_1(p_T \gg Q_s, \eta)$ in the two approaches. The projectile and spectator nuclei are indicated by half circles together with the sign convention of low p_T directed flow v_1.

of the jet quenching pattern, $R_{AA}(\eta, \phi, p_\perp; b > 0)$, and long range rapidity correlations induced by the generic intrinsic rapidity twist of the bulk matter.

At midrapidity, $\eta = 0$, the elliptic asymmetry of the reaction geometry in noncentral $(b > 0)$ $A + A$ reactions leads to a well-known elliptic transverse asymmetry in jet quenching. However, the rapidity twist [1] has no observable effect at midrapidity. At positive rapidities $\eta > 1$, on the other hand, the rapidity twist $\frac{d\langle x_\perp \rangle}{d\eta}$ of the bulk shifts the center of mass away from $\mathbf{x}_\perp = 0$, while at negative rapidities that shift has the opposite sign. In conventional pQCD, collinear factorized $gg \rightarrow gg$ processes predict a jet distribution that is proportional to the local *binary* collision density, $\sigma_{NN} T_B(r_+) T_A(r_-)$, where $r_\pm = \sqrt{(x \pm \frac{b}{2})^2 + y^2}$, and $T_A(\mathbf{x})$ is the Glauber nuclear profile function [1]. The jets are therefore produced symmetrically in azimuthal angle about $\mathbf{x}_\perp = 0$ at all η. The collinear factorized jet density therefore has no rapidity twist as illustrated by the gray ellipse in Fig. 1 labeled pQCD.

As discussed in [1], the bulk matter density is rotated away from the beam axis in the $x - \eta$ plane because the bulk density varies approximately as $\{(Y - \eta) T_A(r_+) + (Y + \eta) T_A(r_-)\}/2Y$, which is not reflection symmetric about $\mathbf{x}_\perp = 0$ away from midrapidity. At $p_T < Q_s$ the CGC model produces approximately the same rapidity twist as wounded nucleon string models since this is a direct consequence of local participant collision scaling of the bulk. However, due to the nonlinear equation determining the local saturation scale $Q_s(\mathbf{x}_\perp, x)$ the bulk surface region may sharpen significantly relative to conventional Wood-Saxon geometry included in $T_A(\mathbf{x}_\perp)$. This surprising change of the bulk surface geometry in the KLN implementation of CGC was first pointed out by Hirano and Nara [15].

As we show below, at higher p_T the simplest KLN implementation of the CGC predicts even greater rapidity twist away from the beam axis than the bulk as shown below and illustrated in Fig. 1. In this paper, we explore the tomographic consequences of such twisted bulk and jet geometries. The KLN/CGC rapidity twist effect turns out to be opposite to that discussed in [1] but depends on the model parameters. Our aim is not to advocate one particular model but to point out observables that may be able to test independently the important features of the geometry that affect collective hydrodynamic observables.

The phenomenological soft + hard and KLN/CGC approaches differ significantly in their predictions for moderately high p_T partons above Q_s. In the former case, the high p_T parton production is calculated from the collinear factorized on shell $gg \rightarrow gg$ approximation of pQCD for hard processes. In the KLN/CGC approach both soft and hard partons are calculated using the k_T factorized off-shell $gg \rightarrow g$ gluon fusion approximation to QCD parton production [16]. The advantage of collinear factorized approximations is that they employ experimentally well-determined nucleon parton structure functions, $xG_{\rm nuc}(x, Q^2)$. In addition, corrections beyond lowest order can be systematically evaluated. The main disadvantage in applications to $A + A$ is that possible nonlinear nuclear effects at low Bjorken x are expected to significantly modify the assumed linear relation $G_A = AG_{\rm nuc}$ in different kinematic regimes.

In contrast, KLN/CGC predictions are based on the convolution of unintegrated nuclear gluon distributions, $\phi_A(x, k_T^2)$ via the Gribov-Levin-Ryskin (GLR) formula [16]. This approach has the advantage of including a nonlinear gluon evolution as $x \rightarrow 0$ via a single gluon saturation scale $Q_s(x, A)$ that can be determined in the weak coupling but strong field approximation. The main disadvantage of this approach is the uncertainty related to how to take the $A \rightarrow 1$ nucleon limit, $\phi_N(x, k_T^2)$. This limit is important phenomenologically because nuclear modification is measured relative to the $N + N$ baseline. In addition, near the nuclear surface the participant nucleon density decreases rapidly and Q_s is driven below 1 GeV where the weak coupling strong field approximations may fail. Since the surface regions in finite $A + A$ contribute significantly ($\sim 10\%$–20%) to the global $dN/d\eta$, it is important to devise experimental tests sensitive to the low A limit of CGC. Unlike the integrated parton distributions, there is no general consensus yet on the form of ϕ_N [17]. Additional theoretical uncertainty is associated with the unknown applicability range of the first order GLR k_T factorization formulation [16] as compared to proposed higher order nonlinear generalizations [18].

Even though there is no consensus yet on the proper parametrization of $\phi_A(x, Q^2)$, we will utilize the KLN parametrization because of its ability to reproduce the integrated bulk properties at RHIC. Recent work on the CGC concentrates on other features of saturation physics like geometric scaling and the CGC anomalous dimension [19,20]. Furthermore, there has been progress on the effect of the onset of DGLAP evolution [21]. While these ongoing improvements of the CGC theory are likely to change the numerical results here, we use KLN/CGC for illustrative purposes.

II. THE LOCAL GLUON DISTRIBUTION

The local generalization of k_T-factorization GLR formula [16] and KLN [8] unintegrated distribution functions used by Hirano and Nara [15] is given by

$$\frac{dN_g}{dp_T d^2\mathbf{x}_\perp d\eta} = \frac{4\pi\alpha_s(p_T^2)}{C_F}\frac{1}{p_T} \times \int^{p_T} d^2k_T \phi_A\left(x_1, \left(\frac{\vec{k}_T + \vec{p}_T}{2}\right)^2; \mathbf{x}_\perp\right) \times \phi_B\left(x_2, \left(\frac{\vec{k}_T - \vec{p}_T}{2}\right)^2; \mathbf{x}_\perp\right). \quad (1)$$

$C_F = \frac{N_C^2-1}{2N_C}$ and the collinear momentum fractions are given by kinematics, $x_{1,2} = p_T \exp(\pm\eta)/\sqrt{s}$. The running QCD coupling, α_s, is regulated at low momenta by imposing a maximum value $\alpha_{\max} = 0.5$ as implemented in [15]. Note that we use η to denote the rapidity rather than the pseudo rapidity as in [1].

$\phi_{A,B}$ are the unintegrated gluon distributions which, in principle, possess a Bjorken x dependence determined by nonlinear evolution equations of the CGC theory [9,10] and their k_T dependence is fixed by a characteristic saturation momentum, $Q_s(x)$. In the McLerran-Venugopalan approach [22] the gluon distribution is suppressed below the saturation scale $\phi_A \sim \log(Q_S^2/k_T^2)$ compared to the perturbative form $\phi_A \sim k_T^{-2}$. We use a parameterization similar to the KLN model approach as used in [15]. We change it for numerical convenience to the following Lorentzian form.

$$\phi_A(x, \vec{k}_T; \mathbf{x}_\perp) = \frac{\kappa}{\alpha(Q_{s,A}^2)} \frac{Q_{s,A}^2}{k_T^2 + Q_{s,A}^2 + \Lambda^2}. \quad (2)$$

The momentum scale $\Lambda = 0.2$ GeV is a regulator for the high rapidity $y > 4.5$ region as in [15]. The constant $\kappa \sim 0.4$ is a parameter set to reproduce $dN_{ch}/d\eta$ measured in the BRAHMS experiment in central collisions (as shown in Fig. 2) [23]. The transverse coordinate dependence is implicit in the saturation momentum determined numerically for each nucleus.

$$Q_{s,A}^2(x, \mathbf{x}_\perp) = \frac{2\pi^2}{C_F}\alpha_s(Q_{s,A}^2) x G_{\text{nuc}}(x, Q_{s,A}^2) T_A(\mathbf{x}_\perp), \quad (3)$$

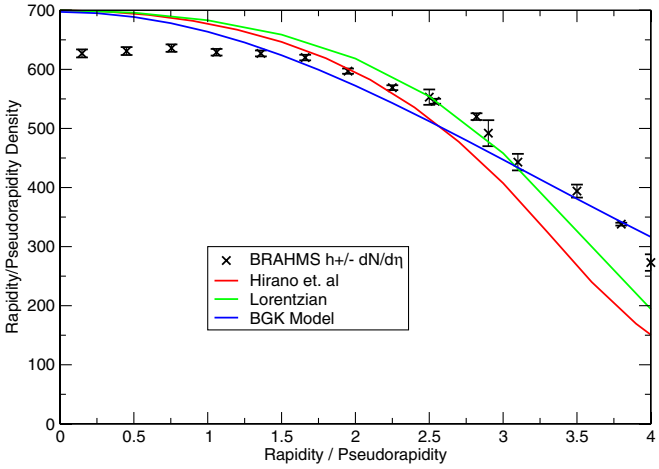

FIG. 2 (color online). The figure shows the pseudorapidity distribution for charged particles as measured by the BRAHMS collaboration [23] with statistical errors shown. Also shown are the rapidity distributions from the Brodsky-Gunion-Kuhn [5] type twist model as in [1], the current CGC model and the CGC model as in Hirano *et al.* [15]. Notice that very similar multiplicity distributions can be reproduced by using all three models. The dip at $\eta \sim 0$ is due to the Jacobian between rapidity and pseudorapidity. The experimental curve is broader than the theory curves, a discrepancy that can be resolved with hydrodynamic evolution.

where T_A is the Glauber profile of nucleus A. We use standard diffuse Woods-Saxon nuclear profiles. The projectile and target nuclei are set up such that the spectator v_1 is positive at forward rapidity.

The perturbative form is used for the nucleonic gluon distribution.

$$xG_{\text{nuc}}(x, Q^2) = K \log\left(\frac{Q^2 + \Lambda^2}{\Lambda^2}\right) x^{-\lambda}(1-x)^n \quad (4)$$

The $x^{-\lambda}$ term accounts for the rapid growth of small Bjorken x gluons while the factor of $(1-x)^n$ was introduced in KLN to account qualitatively for the rapid depletion of gluons as $x \to 1$ outside the small x framework of the CGC model. As in [15], we set $\lambda = 0.2$ and $n = 4$. $K \sim 1.35$ is used to set $\langle Q_s^2(x = 0.01)\rangle \sim 2$ GeV^2 for central collisions at midrapidity.

In Fig. 2 we show the multiplicity distributions generated using the current model as well as the model for Hirano *et al.* (renormalized to $dN/d\eta(\eta = 0) = 700$) [15]. These models are used to reproduce the initial rapidity distribution of gluons needed to approximately predict the charged particle pseudorapidity distribution measured by BRAHMS [23]. We also show the calculation as performed using the BGK model from [1] which qualitatively gives the same results. The data shown in Fig. 2 is a pseudorapidity distribution and is different from the theory curves by a Jacobian factor. It is, however, still broader than the theory curves. This is welcome as we calculate the initial multiplicity distributions which will undergo hydro-

dynamic expansion and thus become broader. A further point to note is that the BGK model calculation shown is different from the one performed in [1]. The BRAHMS data used in [1] has been replaced with alternative BRAHMS measurements that have been better verified by other experiments at RHIC. This changes the twist results of the BGK model appreciably beyond $|\eta| \sim 1$. All BGK calculations shown as comparisons in this paper use the latter data to tune its parameters.

A. Reaction plane spatial distribution

Once the distribution shown in Eq. (1) is evaluated, we are ready to investigate the reaction plane spatial dependence (and hence the intrinsic spatial twist) of the produced gluons as a function of p_T and η. Figure 1 shows the expected twist for low $p_T < Q_s$ and high $p_T > Q_s$ particles in a schematic way. We can now track this asymmetry quantitatively in a more systematic manner. We will notice after our analysis that the anomalous large twist of the high p_T matter is very sensitive to the nuclear edge, an effect that depends on the maximum range of α_s.

The first measure of the asymmetry can be achieved by looking at the prevailing Q_s associated with each nucleus as a function of the transverse horizontal coordinate for different p_T and η. This is shown in Fig. 3. We can easily see in the diagram that the saturation momenta are larger

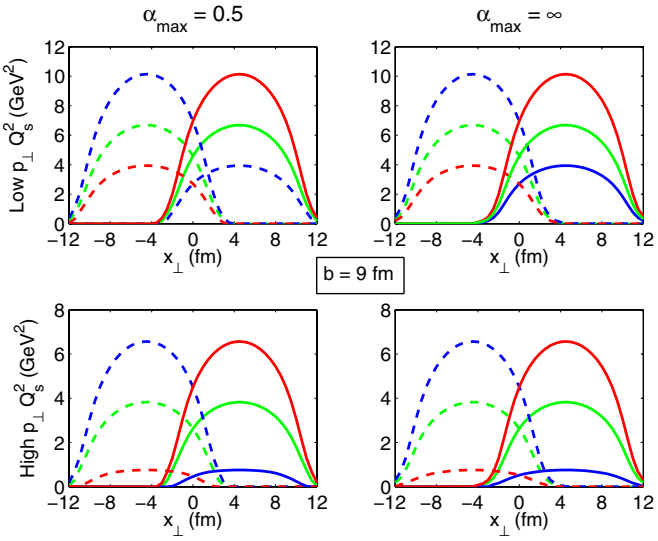

FIG. 3 (color online). The figure shows the squared saturation momentum Q_s^2 as a function of the horizontal transverse coordinate, x_T for different values of p_T and η in the case of a noncentral collision. Low p_T curves are at 1 GeV and high p_T at 8 GeV. Blue curves are at $\eta = 2$, red curves at $\eta = -2$ and green curves at $\eta = 0$. Dashed curves are associated with the target nucleus and solid curves are for the projectile nucleus. Notice that the saturation momenta are smaller for high p_T particles due to the larger Bjorken x values that are probed. The edges of the distribution change depending on the regulator used for α_s. All curves $b = 9$ fm.

for the low p_T particles than for high p_T jet like production. This can be understood from the fact that the momentum fractions are evaluated as $\frac{p_T}{\sqrt{s}} e^{\pm\eta}$ and higher transverse momenta naturally lead to the nuclei being probed at higher momentum fractions. Furthermore, as one moves off midrapidity, the two nuclei are probed at very asymmetric values of Bjorken x due to the exponential factor, thus causing the asymmetry in the final particle production. Note the difference between the Q_s curves with and without a cutoff regulated α_s. Neglecting to regulate α_s allows for a more diffuse nuclear edge. This difference is very small in the low p_T case but is actually appreciable in the high p_T calculations as the Q_s values involved throughout the plane are pretty small and a diffuse edge significantly changes the distribution.

The transverse spatial dependence of the produced matter can be evaluated by using Eq. (1) under various assumptions. To get the low $p_T \approx 1$ GeV distribution we assume that $Q_s^{A,B} \gg p_T, k_T$ while the opposite ordering is assumed for high $p_T \approx 8$ GeV. In either case, we expand Eq. (1) and keep the leading transverse coordinate dependence (via the saturation momenta).

$$\frac{p_T^2 dN_{\text{low}}}{d^2p_T d^2x_T d\eta} \propto f_{\text{low}}(\mathbf{x}_\perp, p_T, \eta) = \frac{p_T^2 - \frac{3}{8}p_T^4\left(\frac{1}{Q_{s,A}^2} + \frac{1}{Q_{s,B}^2}\right)}{\alpha(Q_{s,A}^2)\alpha(Q_{s,B}^2)}$$
$$\frac{p_T^4 dN_{\text{high}}}{d^2p_T d^2x_T d\eta} \propto f_{\text{high}}(\mathbf{x}_\perp, p_T, \eta) = \frac{Q_{s,A}^2 Q_{s,B}^2}{\alpha(Q_{s,A}^2)\alpha(Q_{s,B}^2)} \qquad (5)$$

The functions f_{low} and f_{high} are plotted in Fig. 4 for regulated as well as unregulated α_s. The low $p_T \approx 1$ GeV curves show exactly the twist that we expect and describe earlier in the paper. The produced matter is perfectly symmetric with respect to the transverse coordinate at midrapidity. However, the asymmetric saturation momenta lead to a shift in the produced matter in the transverse plane away from the origin as one moves off midrapidity. Matter at forward rapidity is shifted more towards the projectile nucleus while matter at backwards rapidity is shifted more toward the target. This is very similar to the twist seen in the BGK model and is due to the simple rapidity triangle local wounded nucleon arguments used in [1]. Both the BGK and CGC/KLN models reproduce the low p_T asymmetry because they reproduce simple bulk properties of the nuclear collision.

The high p_T asymmetry of the initial jet production distribution is specific to the KLN/CGC model. Furthermore, the high $p_T \approx 8$ GeV asymmetry in the transverse plane depends on the value of the strong coupling cutoff at low saturation momenta. The figure shows the cases for $\alpha_{\max} = 0.5$ and ∞. The asymmetry is seen to disappear as the cutoff increases and is gone. This asymmetry can be qualitatively understood from the $\mathbf{x}_\perp$ dependence of the saturation momenta and the specific model, Eq. (4) of the nucleonic gluon distribution:

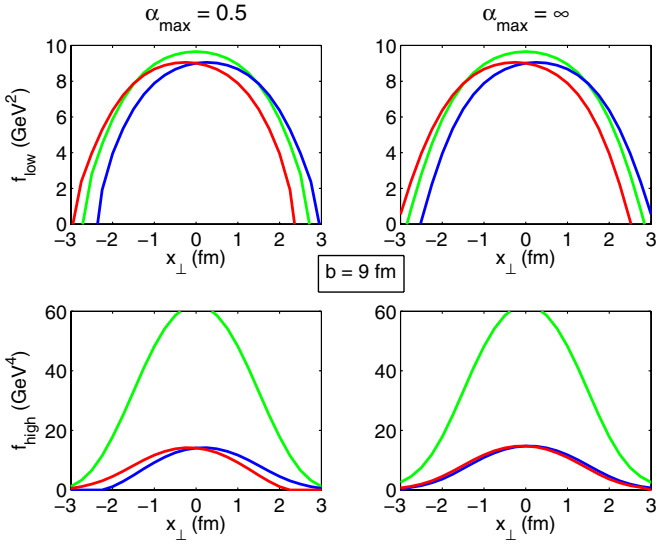

FIG. 4 (color online). The figure shows the functions $f_{\rm low}$ and $f_{\rm high}$ [Eq. (5)] as a function of the transverse coordinate for different values of η. Green curves are at midrapidity, Blue curves are at $\eta = 2$ and red curves are at $\eta = -2$. Low p_T curves are evaluated at 1 GeV and high p_T curves are evaluated at 8 GeV. Note the asymmetry in the curves as one moves off midrapidity, with forward rapidity production biased towards the projectile nucleus and backwards rapidity production biased towards the target. The low p_T asymmetry persists for unregulated α_s but the high p_T asymmetry goes away. All curves $b = 9$ fm.

$$Q_{s,A}^2(r_+)Q_{s,B}^2(r_-) \propto \alpha_s(Q_{s,A}^2)\log\left(\frac{Q_{s,A}^2+\Lambda^2}{\Lambda^2}\right)\alpha_s(Q_{s,B}^2) \times \log\left(\frac{Q_{s,B}^2+\Lambda^2}{\Lambda^2}\right)T_A(r_+)T_B(r_-) \tag{6}$$

Note that the product is proportional to the binary collision distribution, $T_A(r_+)T_B(r_-)$ that is characteristic of conventional collinear factorized formulae used in [1]. However, the prefactor logarithms specific to this for the perturbative gluon distribution and the factor of α_s from the local self consistent KLN determination of Q_s can lead to unexpected novel effects near the surface. While the product of the saturation momenta for $B = A$ appears completely symmetric with respect to reflection of the transverse coordinate $\mathbf{x}_\perp$ with $r_\pm = \sqrt{(x \pm \frac{b}{2})^2 + y^2}$, imposing an $\alpha_{\rm max}$ cutoff on the running coupling breaks this symmetry near the surface because only one of the two saturation momenta tends to vanish. Even though the α_s above cancel with the $1/\alpha_s$ in Eq. (5), the solution to defining saturation Eq. (3) implicitly depends on $\alpha_{\rm max}$. Only far enough from the surface, where the saturation momenta are large enough to insure that both $\alpha_s \geq \alpha_{\rm max}$, is reflection symmetry restored in this model.

A natural question at this point is whether one should try to modify the KLN/CGC parametrization in Eq. (4) and impose the requirement that the product of logarithms and coupling constants in Eq. (6) be set to a constant. Although tempting, this may not be a consistent solution to the problem. The logarithm arising in the function $xG_{\rm nuc}$ is motivated by perturbative DGLAP evolution at high Q^2 and cannot be interpreted simply as $\frac{1}{\alpha_s}$. On the other hand, the α_s in Eq. (3) is motivated by large amplitude saturation physics that must break down near the surface in some way that is still not well understood theoretically.

The point of this paper, however, is not to attempt improvements to current CGC models but to point out how 3D jet tomography could help to test experimentally surface details of initial conditions as illustrated by that model that may lead to important consequences for bulk hydrodynamic phenomena [14]. We therefore use the KLN/CGC parametrization and vary $\alpha_{\rm max}$ for illustration. Further discussions on regulating α_s can be found in [24].

We can investigate the intrinsic spatial twist of the produced matter numerically using Eq. (1). The transverse shift of material away from the origin of the transverse reaction plane is computed via

$$\langle x_\perp\rangle(p_T,\eta) = \frac{\int d^2x_\perp x_\perp dN_g/dp_T d^2x_\perp d\eta}{\int d^2x_\perp dN_g/dp_T d^2x_\perp d\eta}. \tag{7}$$

Here, $x_\perp$ is the transverse coordinate in the direction of the reaction plane, $\vec{b}$. Positive $x_\perp$ points toward the projectile $\eta = Y$ spectator displacement. Figure 5 shows $\langle x_\perp\rangle$ as a

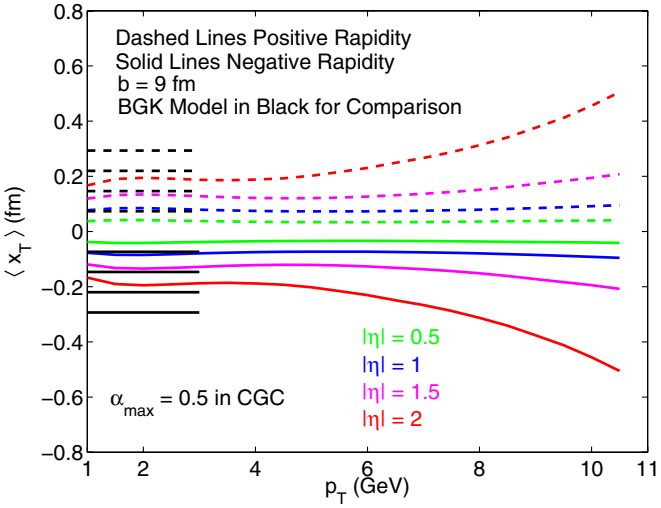

FIG. 5 (color online). The figure shows the average transverse spatial coordinate $\langle x\rangle$ for produced gluonic matter in the Brodksy-Gunion-Kuhn [5] type twist model as in [1], as well as in the current CGC model. Notice that, for BGK, there is no dependence on p_T other than the assumed lack of twist for matter with $p_T > 3$ GeV. The CGC model with $\alpha_{\rm max} = 0.5$, however, has a pronounced increasing rapidity twist for higher $p_T > 6$ GeV.

function of p_T and η for the hybrid Brodsky-Gunion-Kuhn (BGK) [5] participant and binary jet production model (as used in [1]) as well as for the current CGC model (for $b = 9$ fm). The rapidity twist of the BGK model is seen by the increasing $\langle x_\perp \rangle$ as η increases for the bulk $p_T \leq 3$ GeV matter.

While the bulk $\langle x_\perp \rangle$ of the CGC model is similar to the bulk BGK shifts, the high p_T shifts behave oppositely. In the two component BGK approach $\langle x_\perp \rangle = 0$ for high p_T. We show in Fig. 5 that the rapidity twist $(d\langle x_\perp \rangle / d\eta)$ increases at high $p_T > 6$ GeV.

III. TOMOGRAPHY AND THE INVERSE TWIST

Jet tomographic analysis uses the attenuation of jet matter while passing through the bulk in order to gain information about the density profile of the bulk [2]. The observable used most commonly in tomographic analysis is the nuclear modification factor, R_{AA}, which measures the deviation of the produced nucleus-nucleus spectrum, if any, from a simple binary scaled p-p spectrum. The twist effect investigated in the previous section can be observed by looking at the $R_{AA}(p_T, \eta, \phi)$ of jets in the transverse plane.

The azimuthal dependence of R_{AA} will change as a function of η for a given p_T jet due to the differing twist of the jet distribution over η. In order to calculate the $R_{AA}(p_T, \eta, \phi)$ we use a simplified geometric absorption model ([25]) for illustrative purposes. The nuclear modification factor is calculated by,

$$R_{AA}(p_T, \eta, \phi) = \frac{\int d^2\mathbf{x}_\perp e^{-\mu\chi(\mathbf{x}_\perp, \phi, \eta)} \frac{dN_g}{dp_T d^2\mathbf{x}_\perp d\eta}(p_T, \eta)}{\int d^2\mathbf{x}_\perp \frac{dN_g}{dp_T d^2\mathbf{x}_\perp d\eta}(p_T, \eta)}. \tag{8}$$

where $\mu \sim 0.06$ fm is set to reproduce the observed central $R_{AA}(\eta = 0, b = 0) \sim 0.2$. The opacity, χ, is given by the line integral over the local bulk distribution that attenuates the jet:

$$\chi^{(\alpha)}(\mathbf{x}_\perp, \phi, \eta) = \int d\tau \frac{dN_{\text{bulk}}}{d^2\mathbf{x}_\perp d\eta}(\mathbf{x}_\perp + (\cos\phi, \sin\phi)\tau, \eta)\tau^\alpha \tag{9}$$

The factor of τ^α models the length dependence characteristic of the different types of energy loss. Radiative energy loss in static matter is modeled using $\alpha = 1$, while collisional energy loss is modeled with $\alpha = 0$. In this paper we use the value of $\alpha = 0$ in order to model radiative energy loss in a Bjorken expanding medium. The local bulk density used in calculating the opacity is taken to be the integrated low $p_T < 3$ GeV distribution

$$\frac{dN_{\text{bulk}}}{d^2\mathbf{x}_\perp d\eta} = \int_0^3 dp_T \frac{dN_g}{dp_T d^2\mathbf{x}_\perp d\eta} \tag{10}$$

We can use Eq. (8) to probe the rapidity twist. The antitwist effect of the KLN/CGC can be most easily observed via the first azimuthal Fourier moment of $R_{AA}(p_T, \eta, \phi)$, the directed flow v_1 defined as the following.

$$R_{AA}(p_T, \eta, \phi) = R_{AA}^{\text{ave}}\left(1 + 2\sum_{n=1}^{\infty} v_n \cos(n\phi)\right) \tag{11}$$

Figure 6 shows v_1 as a function of η for different values of the p_T for both the KLN/CGC model and BGK model. The KLN/CGC model is shown for different values of $\alpha_{\max} = 0.5, 1$. Note that for all p_T values there exists a rapidity in the $\alpha_{\max} = 0.5$ model at which the directed flow flips sign. This flip occurs at lower values of the rapidity for higher values of the p_T. The change in sign is a novel prediction using the KLN/CGC model. In conventional factorized QCD jet production, the high p_T v_1 is negative and in the same direction as the low p_T bulk directed flow but increasing with p_T as in hydrodynamics. Both models exhibit long range rapidity anticorrelations of the v_1. Note also that increasing the value of $\alpha_{\max}$ from 0.5 to 1 makes the v_1 tend towards the BGK type model predictions.

We conclude from the variation of the differential directed flow at high p_T *and* $|\eta| > 1$ with $\alpha_{\max}$ and the comparison to previous results from [1] that 3D tomography offers a sensitive test of both bulk and jet spatial initial conditions. Such independent experimental tests of $A + A$ initial conditions are essential to constrain models of initial entropy production such as the CGC and narrow the the range of initial conditions used with hydrodynamic calculations to predict collective flow signatures.

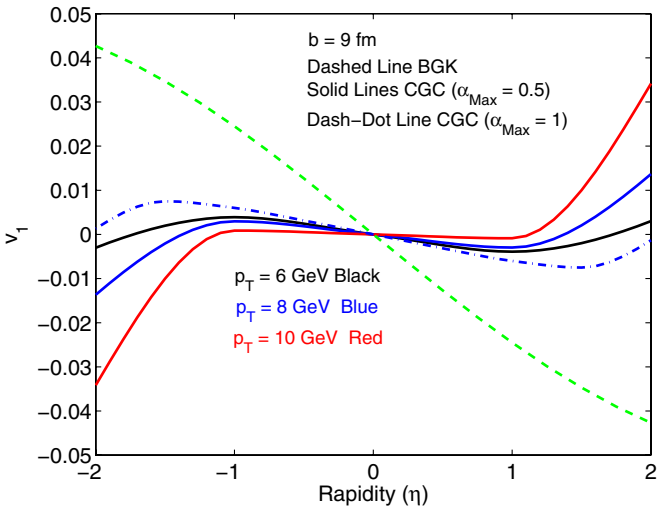

FIG. 6 (color online). The directed flow v_1 as a function of η for different p_T at $b = 9$ fm. Both the CGC model (at $\alpha_{\max} = 0.5, 1$) and BGK model are given for comparison.

ACKNOWLEDGMENTS

Discussions with A. Dumitru, J. Harris, W. Horowitz, D. Kharzeev, L. McLerran, I. Vitev, X. N. Wang and Nu Xu are gratefully acknowledged. This work is supported in part by the United States Department of Energy under Grants No. DE-FG02-93ER40764.

[1] A. Adil and M. Gyulassy, Phys. Rev. C **72**, 034907 (2005).
[2] M. Gyulassy, I. Vitev, X. N. Wang, and B. W. Zhang, nucl-th/0302077; in *Quark Gluon Plasma 3*, edited by R. C. Hwa and X. N. Wang (World Scientific, Singapore, 1998), pp. 123–191; P. Jacobs and X. N. Wang, Prog. Part. Nucl. Phys. **54**, 443 (2005).
[3] B. B. Back *et al.* (PHOBOS Collaboration), Phys. Rev. Lett. **93**, 082301 (2004).
[4] I. Arsene *et al.* (BRAHMS Collaboration), Phys. Rev. Lett. **94**, 032301 (2005).
[5] S. J. Brodsky, J. F. Gunion, and J. H. Kuhn, Phys. Rev. Lett. **39**, 1120 (1977).
[6] B. Andersson, G. Gustafson, and B. Nilsson-Almqvist, Nucl. Phys. **B281**, 289 (1987).
[7] X. N. Wang and M. Gyulassy, Phys. Rev. D **44**, 3501 (1991); Comput. Phys. Commun. **83**, 307 (1994).
[8] D. Kharzeev, E. Levin, and M. Nardi, Nucl. Phys. **A730**, 448 (2004); **A743**, 329(E) (2004); **A747**, 609 (2005).
[9] E. Iancu, A. Leonidov, and L. D. McLerran, Nucl. Phys. **A692**, 583 (2001).
[10] J. P. Blaizot and F. Gelis, Nucl. Phys. **A750**, 148 (2005).
[11] M. Gyulassy and L. McLerran, Nucl. Phys. **A750**, 30 (2005); See also articles by T. D. Lee, J. P. Blaizot, B. Muller, E. Shuryak, H. Stöcker, and X. N. Wang, Nucl. Phys. **A750**, 1 (2005).
[12] K. Adcox *et al.* (PHENIX Collaboration), Nucl. Phys. **A757**, 184 (2005); B. B. Back *et al.* (PHOBOS Collaboration), Nucl. Phys. **A757**, 28 (2005); I. Arsene *et al.* (BRAHMS Collaboration), Nucl. Phys. **A757**, 1 (2005); J. Adams *et al.* (STAR Collaboration), Nucl. Phys. **A757**, 102 (2005).
[13] T. Hirano and M. Gyulassy, nucl-th/0506049.
[14] T. Hirano, U. W. Heinz, D. Kharzeev, R. Lacey, and Y. Nara, nucl-th/0511046.
[15] T. Hirano and Y. Nara, Nucl. Phys. **A743**, 305 (2004).
[16] L. V. Gribov, E. M. Levin, and M. G. Ryskin, Phys. Rep. **100**, 1 (1983); Phys. Lett. B **100B**, 173 (1981); E. Laenen and E. M. Levin, Annu. Rev. Nucl. Part. Sci. **44**, 199 (1994).
[17] B. Andersson *et al.* (Small x Collaboration), Eur. Phys. J. C **25**, 77 (2002); A. Szczurek, Acta Phys. Pol. B **34**, 3191 (2003); L. Lonnblad and M. Sjodahl, J. High Energy Phys. 05 (2005) 038.
[18] N. N. Nikolaev and W. Schafer, Phys. Rev. D **71**, 014023 (2005).
[19] D. Kharzeev, Y. V. Kovchegov, and K. Tuchin, Phys. Rev. D **68**, 094013 (2003); D. Kharzeev, Y. V. Kovchegov, and K. Tuchin, Phys. Lett. B **599**, 23 (2004).
[20] E. Iancu, K. Itakura, and L. McLerran, Nucl. Phys. **A708**, 327 (2002).
[21] A. Dumitru, A. Hayashigaki, and J. Jalilian-Marian, Nucl. Phys. **A765**, 464 (2006); hep-ph/0512129.
[22] L. D. McLerran and R. Venugopalan, Phys. Rev. D **49**, 2233 (1994); **49**, 3352 (1994); **50**, 2225 (1994).
[23] I. Arsene *et al.* (BRAHMS Collaboration), Phys. Rev. Lett. **88**, 202301 (2002).
[24] D. Kharzeev, E. Levin, and M. Nardi, Phys. Rev. C **71**, 054903 (2005).
[25] A. Drees, H. Feng, and J. Jia, Phys. Rev. C **71**, 034909 (2005).